J. Fluid Mech. (2005), *vol.* 537, *pp.* 35–53.
doi:10.1017/S0022112005005124 Printed in the United Kingdom

Precipitate formation in a porous rock through evaporation of saline water

By GEORGE G. TSYPKIN[1] AND ANDREW W. WOODS[2]

[1]Institute for Problems in Mechanics, RAS, Moscow, Russia

[2]BP Institute, University of Cambridge, Madingley Rise, Cambridge, CB3 0EZ, UK

(Received 21 July 2004 and in revised form 14 February 2005)

We examine the motion of a high-pressure aqueous solution, through a low-permeability fracture, towards a low-pressure well. As the liquid decompresses in the fractures it expands, and for sufficiently high initial temperature the liquid reaches the boiling point. A vaporization front then develops, so that vapour issues from the well. As the fluid evaporates near the well, the salt concentration of the residual fluid increases. If the salt concentration increases beyond the saturation limit, then the evaporation leads to precipitation of salt in the fracture. We find a new family of self-similar solutions to describe the boiling and precipitation in a single idealized fracture, which at long times remains approximately isothermal owing to the cross-fracture heat transfer. The solutions describe the mass of salt that precipitates as a function of the initial salt concentration, the reservoir temperature and pressure, and the well pressure. In fact, this family of self-similar solutions is multi-valued: we identify a liquid-advection-dominated regime, in which the boiling front advances slowly and the fracture porosity decreases significantly, and a boiling-dominated regime, in which the boiling front advances more rapidly, and less precipitate forms at each point in the fracture. As the pressure difference between the well and the far field reservoir increases, these solutions converge, and eventually coincide. Beyond this critical point, there is no similarity solution, since the advective flux of salt from the far-field would produce more precipitate than can be taken up in the fracture adjacent to the boiling front. Instead, the rock will become fully sealed through precipitation, thereby suppressing flow into the well. We extend the model to show that an analogous result also occurs within an extensive porous layer. However in that case, the system is not isothermal; instead, the heat flux is supplied in the direction of flow, while the cross-flow heat flux is small. We discuss the relevance of the work to the natural venting of steam in high-temperature geothermal systems.

1. Introduction

Many naturally occurring geothermal systems are saturated with aqueous saline solutions at high temperature and pressure. If a fracture or other opening develops in such a formation, for example following geologic or tectonic activity, then the fluid will expand and migrate to this region of lower pressure. The region of decompression may extend over a large lateral distance, and if the fluid is sufficiently hot, it may reach conditions for boiling. In that case, an advancing evaporation front will develop within the rock (Tsypkin & Woods 2004). Since the dissolved salts are typically insoluble in the vapour phase, the concentration of salts in the fluid will increase in the vicinity of the front. If the salt concentration increases above the solubility limit, then a fraction

of the salt may precipitate in the rock, reducing the permeability of the formation (Phillips 1991). Over geological time scales this natural process may have a key role in the formation of some geothermal mineral deposits.

The purpose of this work is to explore some of the controls on the dynamics of this precipitation process. Although there has been some numerical modelling of these processes, it is a difficult task for numerical solution, owing to the large difference in scales between the compositional and thermal diffusivities (Battistelli, Calore & Pruess 1995, 1997). We have therefore broken the study into a series of elements, to build basic insight. First, we examine the simplified one-dimensional problem of boiling and salt precipitation within a single low-permeability fracture which is initially saturated with water at high pressure. This work exposes many of the key controls on the boiling and precipitation process and forms the heart of the paper. However, we then extend the analysis to the case of boiling and salt precipitation in a porous layer, rather than a fracture, to show how some of the key principles carry over to this more involved problem.

The paper is arranged as follows. In §§ 2, 3 and 4 we focus on the case of flow in a low-permeability fracture, bounded by impermeable rock, driven by the sudden decompression at a well which intersects the fracture. In this situation, we expect that at long times, the fracture will become approximately isothermal. This may be understood by considering the heat budget within the fracture. First, the heat flux from the walls of the fracture depends on the thickness of the conductive boundary layer, which increases as $(at)^{1/2}$ where a is the thermal diffusivity and t is time. Secondly, the decompression of the liquid within the fracture (Tsypkin & Woods 2004) leads to a diffusive flux of fluid at the well-bore and hence we expect the boiling front to migrate along the fracture a distance which scales as $(\kappa t)^{1/2}$ after time t where κ is the effective pressure diffusion coefficient. Therefore, the heat flux which can be supplied to the fracture from the bounding walls for vaporization scales as $(\kappa a)^{1/2}t$. However, the mass of liquid in the fracture which can take up this heat flux in the form of latent heat only scales as $w(\kappa t)^{1/2}$ per unit length, where w is the width of the fracture. As a result, for times in excess of w^2/a, the fracture temperature increases towards that of the far field. We examine this long-time limit in which the system is approximately isothermal, even at the vaporization front. We discover that there is a multi-valued family of similarity solutions to describe the flow and vaporization, when the effect of precipitation on reducing the permeability of the fracture are included.

In § 5, we develop the analysis for application to a one-dimensional vaporization front within a uniform porous layer. In this different case, the temperature decreases in the direction of flow in order to supply heat to the boiling front (Tsypkin & Woods 2004). However, again we find a family of similarity solutions for low-pressure reservoirs, and we find that there are again two solution branches. The two limits of the isothermal fracture and the porous media which includes temperature variations are somewhat analogous to isothermal and adiabatic processes. Finally, in the discussion we explore the geological implications of our results.

2. Boiling at constant temperature in a fracture

The primary objective in the present work is to investigate the salt precipitation process associated with a vaporization front in a permeable fracture or porous matrix. For simplicity in this section we focus on the idealized problem of isothermal boiling within a fracture, as motivated in the introduction. We assume the fracture is sufficiently narrow that the flow is of low Reynolds number, and hence may be

described by Darcy's law with the effective permeability being related to the width of the fracture.

2.1. *Vaporization of pure water*

Vaporization occurs within the geothermal reservoir if the pressure P_w in the well-bore is less than the saturation pressure $P_f(T_0)$. Vaporization then occurs at constant temperature and pressure $P_f(T_0)$ where the initial temperature of the reservoir is T_0.

In the water zone, the pressure evolves according to Darcy's law and the equation for mass conservation, and has the form

$$\frac{\partial P}{\partial t} = \kappa_1 \Delta P \qquad \text{where} \quad \kappa_1 = \frac{k}{\phi \alpha_w \mu_w} \tag{2.1}$$

where k is the permeability and ϕ the porosity of the low-permeability fracture, while μ is the viscosity and α_w the water compressibility coefficient. We assume that the vapour behaves as a perfect gas and that it migrates through the porous rock according to Darcy's law and the conservation of mass (Tsypkin & Woods 2004)

$$\frac{\partial P}{\partial t} = \frac{k}{\phi \mu_v} (\text{grad } P)^2 + \frac{k}{\phi \mu_v} P \Delta P. \tag{2.2}$$

The subscripts w and v refer to the properties of the water and vapour respectively.

At the vaporization front, mass conservation takes the form

$$\phi (\rho_w - \rho_{v*}) V_n = Q_{vn} - Q_{wn} \tag{2.3}$$

where V is the velocity of the vaporization front, n denotes the direction normal to the front and Q_j denotes the mass flux for water ($j = w$) and vapour ($j = v$), as defined from Darcy's law

$$Q_j = \rho_j \frac{k}{\mu_j} \text{ grad } P. \tag{2.4}$$

Substituting the mass fluxes into (2.3) we obtain the relation

$$\phi \left(1 - \frac{\rho_{v*}}{\rho_w}\right) V_n = \frac{k}{\mu_v} \frac{\rho_{v*}}{\rho_w} (\text{grad } P)_{n-} - \frac{k}{\mu_w} (\text{grad } P)_{n+} \tag{2.5}$$

where the pressure P_* and vapour density ρ_{v*} at the vaporization surface are defined by relations

$$P_f(T_0) = P_*(T_0), \quad \rho_{v*} = \frac{P_f}{RT_0}. \tag{2.6}$$

Here $P = P_*(T_*)$ is the Clausius–Clapeyiron relation which determines the vaporization pressure as a function of the vaporization temperature. We use the following approximation for the Clausius–Clapeyron curve which is valid for pressures of order 10^5–10^7 Pa:

$$\ln \frac{P_*}{P_a} = A + \frac{B}{T_*}, \qquad A = 12.512, \quad B = -4611.73, \quad P_a = 10^5 \text{ Pa}. \tag{2.7}$$

2.2. *Quasi-stationary approximation for the vapour region*

In the case of a vaporization front which migrates slowly through the fracture away from the well-bore, the pressure distribution across the vapour zone is able to respond rapidly to changes in the mass flux and location of the front, owing to the relatively low density of the vapour. As a result, the pressure distribution in this zone is expected

to be quasi-steady. This result may be established more formally by comparison of the magnitude of the different terms in the pressure diffusion equation. Without loss of generality we set $V_n > 0$ and, using the fact that the velocity of the front and the velocity of the fluids have opposite directions, then from boundary condition (2.5) we have

$$\phi\left(1-\frac{\rho_{v*}}{\rho_w}\right)V_n < \frac{k}{\mu_v}\frac{\rho_{v*}}{\rho_w}(\text{grad } P)_{n-}. \tag{2.8}$$

Assuming that the reservoir temperature is much less than the critical temperature for water, then $\rho_v \ll \rho_w$. Thus if L_P is the typical length scale for the pressure variations then

$$\phi\frac{L_P}{t} < \frac{k\hat{P}}{\mu_v}\frac{\rho_{v*}}{\rho_w}\frac{1}{L_P} \tag{2.9}$$

and owing to the relatively small value for the vapour density, we obtain

$$\frac{L_P^2}{t} \ll \frac{k\hat{P}}{\phi\mu_v} \qquad \text{or} \qquad \frac{L_P^2}{t}\frac{\phi\mu_v}{k\hat{P}} \ll 1. \tag{2.10}$$

The term on the left-hand side of equation (2.2) has order $\hat{P}/t$ and both terms on the right-hand side have order $k\hat{P}^2/(\phi\mu_v L_P^2)$. Thus, the ratio of term on the left-hand side to any term on right-hand side is equal to $(L_P^2/t)(\phi\mu_v/k\hat{P})$. Then, according to (2.10), the term on left-hand side can be neglected and we obtain the approximate relation for the vapour pressure

$$(\text{grad } P)^2 + P\Delta P = 0. \tag{2.11}$$

2.3. *Similarity solution*

We consider one-dimensional flow in an unbounded constant-temperature fracture, located in the half-space $x > 0$. We assume that at the extraction well, $x = 0$, the pressure has value P_w. Thus, the boundary and initial conditions have the form

$$x = 0: \quad P = P_w, \qquad t = 0: \quad P = P_0. \tag{2.12}$$

This problem admits a similarity solution

$$P = P(\zeta), \quad \zeta = \frac{x}{2\sqrt{\kappa t}}, \quad X(t) = 2\gamma\sqrt{\kappa t}, \qquad \kappa = \alpha_w^2 P_f^2 \kappa_1. \tag{2.13}$$

In the vapour region $0 < \zeta < \gamma$, the pressure distribution is given by

$$P(\zeta) = \sqrt{(P_w)^2 + \left(P_f^2 - P_w^2\right)\frac{\zeta}{\gamma}}, \tag{2.14}$$

while the pressure distribution in the water region $X(t) < x < \infty$ is derived from equation (2.1) and has the form

$$P(\zeta) = P_0 + (P_f - P_0)\frac{\text{erfc}(\alpha_w P_f \zeta)}{\text{erfc}(\alpha_w P_f \gamma)}. \tag{2.15}$$

The unknown parameter γ can be found if we substitute solutions (2.14) and (2.15) into the boundary condition (2.5) at the vaporization front leading to the

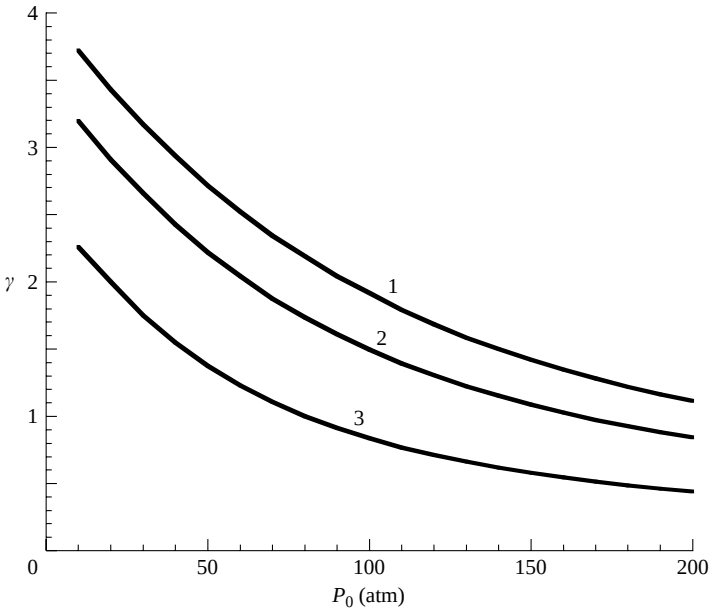

FIGURE 1. Vaporization of the fresh water. Variation of dimensionless velocity of the front as a function of the reservoir pressure for the different values of the well pressure. $T_0 = 450$ K, $\phi = 0.2$; curve 1, $P_w = 4 \times 10^5$ Pa; 2, $P_w = 6 \times 10^5$ Pa; 3, $P_w = 8 \times 10^5$ Pa.

transcendental equation

$$\left(1 - \frac{\rho_{v*}}{\rho_w}\right)\gamma = -\frac{1}{\sqrt{\pi}}\left(\frac{P_0}{P_f} - 1\right)\frac{\exp\left(-\gamma^2\alpha_w^2 P_f^2\right)}{\operatorname{erfc}(\gamma\alpha_w P_f)} + \frac{\rho_{v*}}{\rho_w}\,\frac{\mu_w}{\mu_v}\,\frac{1}{4\alpha_w P_f \gamma}\left(1 - \frac{P_w^2}{P_f^2}\right). \tag{2.16}$$

It may be seen that the transcendental equation for the new variable γ does not depend on the permeability k. This rationalizes the result that the velocity of the vaporization front increases with the permeability as $\sqrt{k}$.

In figure 1, we present a series of calculations illustrating the variation of the velocity of the boiling front as a function of the far-field pressure. Curves are given for three different values of the well pressure. Notice that even for very large values of the reservoir pressure and hence liquid flux, the velocity of the front remains greater than zero.

Equation (2.16) shows that if the reservoir pressure P_0 increases then the velocity of the front γ becomes smaller and the asymptotic decay of γ with P_0 follows from the relation

$$-\frac{1}{\sqrt{\pi}}\left(\frac{P_0}{P_f} - 1\right) + \frac{\rho_{v*}}{\rho_w}\,\frac{\mu_w}{\mu_v}\,\frac{1}{4\alpha_w P_f \gamma}\left(1 - \frac{P_w^2}{P_f^2}\right) = 0. \tag{2.17}$$

This relation identifies that, even with very large initial reservoir pressure, there is always a vaporization front although the velocity of the front may be very small.

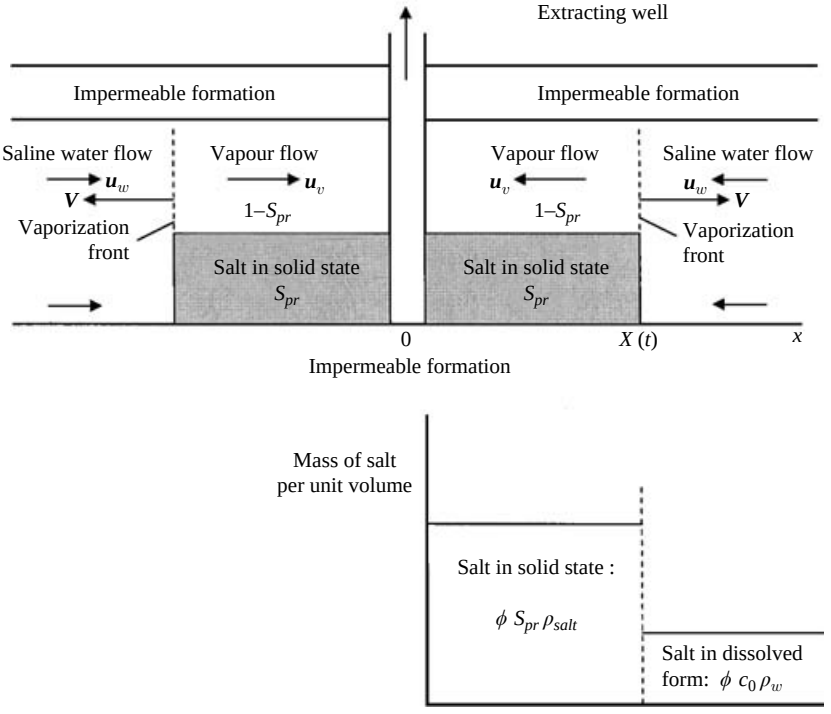

FIGURE 2. Schematic configuration of the boiling front and salt precipitation zones adjacent to the low-pressure well within the fracture.

3. Salt precipitation in an isothermal fracture

In the case in which the liquid consists of an aqueous solution, then, as the liquid boils, it may precipitate some salt. Salt in a solid state occupies some part of the volume of the porous space within the fracture, which we denote as S_{pr}. The fluid then occupies the remaining part $1 - S_{pr}$. Thus, the mass of fluid per unit volume of porous medium is equal to $\phi(1 - S_{pr})\rho_{fluid}$ and the mass of salt in solid state is equal to $\phi S_{pr}\rho_{salt}$. Such precipitation may reduce the permeability of the fracture near the well. As a result, for a given liquid flux from the far field, the extent of the boiling zone is reduced, in order to drive the vapour flux to the well from the vaporization front (figure 2).

Quantification of the change in permeability of the fracture depends on the structure of the pore space, including any roughness elements or other grains, and on the distribution of the precipitate within the matrix (Phillips 1991; Battistelli *et al.* 1995). Here, we use a parametric relation to describe this change in permeability with the mass of precipitate given by

$$k_{-} = k_0 \frac{1 - \exp(\vartheta\phi(1 - S_{pr}))}{1 - \exp(\vartheta\phi)} \equiv k_0 K(S_{pr}) \tag{3.1}$$

where ϑ is a coefficient which accounts for different changes in the permeability as a result of precipitation (figure 3).

3.1. *Asymptotic estimate for a clogging point*

Some important features of the salt precipitation process can be illustrated in the limiting case in which the velocity of the vaporization front is small. For a given flow

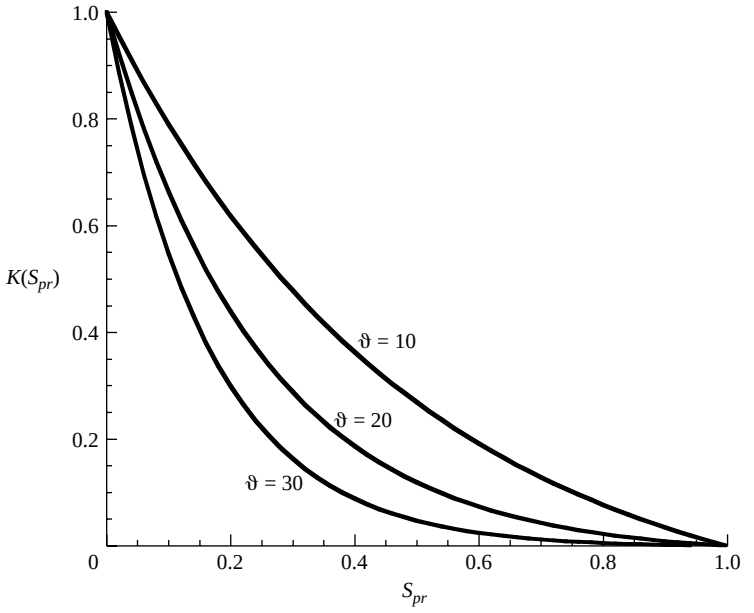

FIGURE 3. Dimensionless permeability as a function of S_{pr} for three different values of parameter ϑ.

rate from the far field, if the fluid has salt concentration c_0 (which is defined as mass of salt per unit mass of solution), then the mass of salt precipitated per unit volume in the fracture can be found from the mass conservation law. We first assume that all salt precipitates at the vaporization front and that there is no salt diffusion ahead of the front. Thus, we obtain

$$m_{salt} \equiv \phi \rho_{salt} S_{pr} = c_0 \frac{Q_w}{V} + \phi \rho_w c_0. \tag{3.2}$$

For a self-similar flow, for which the boiling front advances at a rate $t^{-1/2} V_0$ the fluxes vary as $Q_w = t^{-1/2} Q_{w0}$ and $Q_v = t^{-1/2} Q_{v0}$ where Q_{w0}, Q_{v0} are constants. We therefore find that the relation for the vapour flux may be simplified to the form

$$Q_{vo} = \rho_{v*} \frac{k_0 K(S_{pr})}{\mu_v} \frac{\delta P}{V_0} \tag{3.3}$$

where δP is the fixed difference in pressure between the boiling front and the well. Combining relations (2.3) and (3.2) we find that

$$\phi(\rho_{salt} S_{pr} - c_0 \rho_{v*}) = c_0 \frac{Q_{v0}}{V_0}. \tag{3.4}$$

As $\rho_{salt} S_{pr} > \rho_w c_0$ and we assumed that $\rho_w \gg \rho_v$ the second term on the left-hand side can be ignored and the last relation becomes

$$\phi \rho_{salt} S_{pr} = c_0 \frac{Q_{v0}}{V_0}. \tag{3.5}$$

Substituting V_0 from (3.3) into (3.5) we have

$$Q_{vo}^2 = \frac{\phi \rho_{v*} \rho_{salt} k_0 \, \delta P}{c_0 \mu_v} S_{pr} K(S_{pr}). \tag{3.6}$$

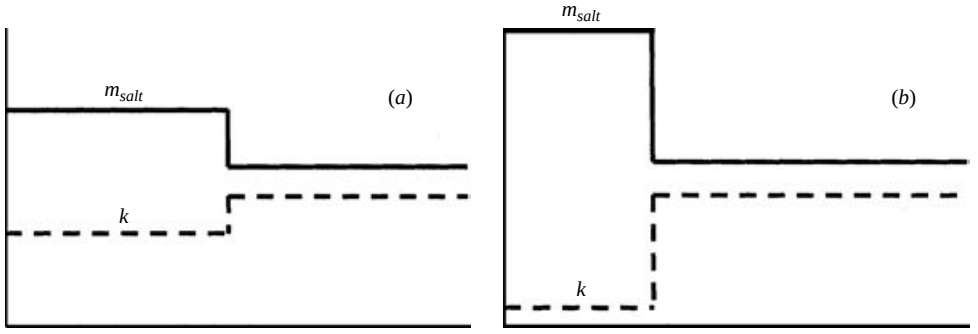

FIGURE 4. Schematic distribution of the mass of salt and of the permeability for the two types of solution: (*a*) fast flow; (*b*) slow flow.

Since the permeability decreases as the mass of salt precipitated increases, then the quantity $S_{pr}K(S_{pr})$ may vary non-monotonically with S_{pr}. Indeed, it is likely to be very small for both small and large values of S_{pr}, corresponding to the cases of a very small mass of precipitate and a large mass of precipitate which nearly clogs the fracture. For intermediate values, the value of $S_{pr}K(S_{pr})$ is likely to be larger and we expect that there is some intermediate value S^*_{pr}, such that $K(S^*_{pr}) = -S^*_{pr}K'(S^*_{pr})$, corresponding to a local maximum. Hence, for $Q_{v0} < Q_{v0}(S^*_{pr})$, there are two possible solutions for S_{pr} and hence V_0 for the given value of Q_{v0}, with the other parameters being fixed. This is a remarkable difference from the case with no precipitation, for which there is a unique solution for the speed of advance of the vaporization front. Now, for a given liquid flow from the far field, we have a slow boiling front which leads to a substantial mass of precipitate, and a fast boiling front which leads to much less precipitate per unit mass of rock. Figure 4 shows a schematic of the two possible flow solutions for a given liquid flux. A fast flow with a small amount of precipitate and a wide vapour zone, and a slow flow with a large amount of precipitate and a much narrowed vapour zone.

This result also identifies that with precipitation there is a maximum liquid flow rate for which is it possible to achieve a self-similar solution. For larger values of liquid flux, the mass of precipitate advected from the far field is too great, and instead the fracture is expected to clog up. Notice from equation (2.3) that the maximal value of the vapour flux is larger than the maximal value of the water flux and that the difference between the fluxes is proportional to the velocity V of the vaporization front. If V tends to zero then Q_v tends to Q_w. The maximal value of water flux Q^*_w which defines the clogging point is reached for $S_{pr} = S^*_{pr}$. Therefore the value $S = S^*_{pr}$ which defines the local maximum of the function $S_{pr}K(S_{pr})$ may be used as an asymptotic estimate for the point at which clogging first occurs and $V \to 0$. This property will be illustrated on the following pages.

3.2. *Quantitative analysis of the multiple solutions*

We now explore these multi-valued solutions in more detail, by extending the quantitative model to account for salt precipitation. The salt distribution is governed by the mass conservation equation

$$\phi \frac{\partial c}{\partial t} + \boldsymbol{v}_w \text{ grad } c = \phi \text{ div } (D \text{ grad } c). \tag{3.7}$$

Equation (3.7) can be simplified by noting that in the water region there is a large difference between the typical length scales, L_c and L_P, over which the salt concentration and pressure fields vary:

$$L_c \sim \sqrt{Dt} \quad \text{and} \quad L_P \sim \sqrt{\kappa_1 t}. \tag{3.8}$$

Thus, comparing the ratio of the term on the right-hand side of equation (3.7) with the second term on left-hand side, for typical values of pressure $\hat{P}$ and salt concentration $\hat{c}$, we have

$$\phi D \frac{\hat{c}}{L_c^2} \Big/ \frac{k}{\mu_w} \frac{\hat{P}}{L_P} \frac{\hat{c}}{L_c} \sim \frac{\phi \mu_w \sqrt{\kappa_1 D}}{k \hat{P}} \equiv \frac{P_f}{\hat{P}} \sqrt{\frac{D}{\kappa}} = \chi. \tag{3.9}$$

If the dimensionless parameter $\chi \ll 1$, then the diffusive transport of salt can be ignored relative to the advective transport and, substituting the flow rate $\boldsymbol{v}_w$ from the Darcy's law, the salt transport equation has the form

$$\frac{\partial c}{\partial t} - \frac{k}{\phi \mu_w} \text{grad } P \text{ grad } c = 0. \tag{3.10}$$

We assume that the salt precipitates across a narrow front that coincides with the vaporization front. The boundary conditions across this front may be found using the conservation of mass for the solution and the salt, including the reduction in the porosity and permeability of the vapour region due to the formation of a salt deposit with density ρ_{salt}. Meanwhile the permeability in the vapour region is a known function of S_{pr}. The boundary condition for the mass of solution has the form

$$\left[\rho_w - S_{pr}\rho_{salt} - (1 - S_{pr})\rho_{v*}\right] V_n = -\rho_{v*} u_{vn-} + \rho_w u_{wn+}. \tag{3.11}$$

Neglecting the salt diffusion, we find that the conservation of salt across the vaporization front has the form

$$\left(S_{pr}\rho_{salt} - c_+ \rho_w\right) V_n = -\rho_w c_+ u_{wn+}. \tag{3.12}$$

Relations (3.11) and (3.12) are supplemented by the Clausius–Clapeyron relation (2.7) which determines the vaporization pressure as a function of the initial temperature. Since the vaporization temperature is only weakly dependent on the salt concentration, we neglect this effect in the present analysis.

In order to illustrate the physical mechanism of salt precipitation we rewrite equation (3.12) as

$$S_{pr} = \frac{\rho_w}{\rho_{salt}} c_+ \left[1 + \frac{k}{\phi \mu_w} \frac{1}{V_n} (\text{grad } P)_{n+}\right]. \tag{3.13}$$

The character of the salt precipitation process described by (3.13) may be determined by the terms on the right-hand side. The first term describes the amount of salt that precipitates when molecules of salt are motionless relative to the fracture. The second term describes the salt transport caused by fluid motion. If the front velocity V_n is sufficiently small then the salt accumulates in the solid phase owing to advective salt transport towards the well-bore.

The initial condition for the salt concentration has the form

$$t = 0: \quad c = c_0. \tag{3.14}$$

3.3. *Similarity solution*

As there is no external length-scale in the problem, the system admits similarity solutions for constant initial pressure and salt concentration and a fixed lower pressure in the well

$$P = P(\zeta), \quad c = c(\zeta), \quad \text{where } \zeta = \frac{x}{2\sqrt{\kappa t}}, \tag{3.15}$$

in which the location of the boiling front is given by

$$X(t) = 2\,\gamma\sqrt{\kappa t}. \tag{3.16}$$

Similarity solutions for the vapour and water pressure have the form (2.14) and (2.15). The similarity solution for the salt concentration has the trivial form $c \equiv c_0$.

By combining the solutions (2.14), (2.15) and the trivial solution $c \equiv c_0$ with the boundary conditions (3.11), (3.13) we obtain the following system of two transcendental equations for the quantities γ and S_{pr} which determine the similarity solution:

$$\left[1 - S_{pr}\frac{\rho_{salt}}{\rho_w} - (1 - S_{pr})\frac{\rho_{v*}}{\rho_w}\right]\gamma = -\frac{1}{\sqrt{\pi}}\left(\frac{P_0}{P_f} - 1\right)\frac{\exp\left(-\gamma^2\alpha_w^2 P_f^2\right)}{\operatorname{erfc}(\gamma\alpha_w P_f)} + \frac{\rho_{v*}}{\rho_w}\,\frac{\mu_w}{\mu_v}\,\frac{K(S_{pr})}{4\alpha_w P_f \gamma}\left(1 - \frac{P_w^2}{P_f^2}\right), \tag{3.17}$$

$$S_{pr} = \frac{\rho_w}{\rho_{salt}}c_0\left[1 + \frac{1}{\sqrt{\pi}\gamma}\left(\frac{P_0}{P_f} - 1\right)\frac{\exp\left(-\gamma^2\alpha_w^2 P_f^2\right)}{\operatorname{erfc}(\gamma\alpha_w P_f)}\right]. \tag{3.18}$$

In figure 5, we compare the values of γ predicted by this model for the rate of propagation of the boiling front with the predictions of the model in the case in which the precipitation is neglected. The solution curve is very different with precipitation, as expected from the argument at the start of this section. We find that there are two solutions for small values of the far-field pressure and hence liquid flux, but that as the reservoir pressure increases, these two solutions eventually meet, and for large values of the pressure, there is no solution. Curves are given for three values of the well pressure. The maximum values of the reservoir pressure may be determined from the root of the relation $S_{pr}K'(S_{pr}) = -K(S_{pr})$, as described above.

In conjunction with figure 5, in figure 6 we illustrate the variation of the mass of precipitate in the pore space as a function of the far-field pressure, for the same three values of the well pressure. Here, one may see how the slow boiling solution has a much higher mass of precipitate per unit volume of rock.

The criterion

$$\frac{\mathrm{d}}{\mathrm{d}S_{pr}}S_{pr}K(S_{pr}) = 0 \tag{3.19}$$

which determines the critical value of salt precipitate in the fracture and hence the maximum liquid flux, for which there is a self-similar solution, may be compared with the numerical solution. In figure 7, the curve $S_{pr}K(S_{pr})$ is shown as a function of S_{pr}, and the critical value for S_{pr} at which (3.21) is satisfied occurs for $S_{pr} \approx 0.24$. In this figure we also show the critical value S_{pr}^* as calculated from the complete similarity solution for three values of the salt concentration, 0.01, 0.03 and 0.12. It is seen that the exact value depends on the initial salt concentration. For small initial concentration, a

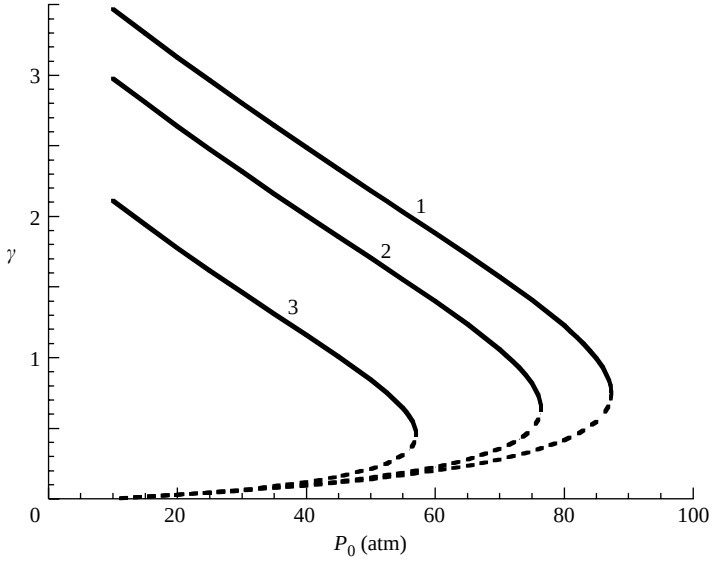

FIGURE 5. Variation of dimensionless velocity of the front as a function of the reservoir pressure for the different values of the well pressure. $T_0 = 450$ K, $\phi = 0.2$, $c_0 = 0.1$, $\vartheta = 20$: curve 1, $P_w = 4 \times 10^5$ Pa; 2, $P_w = 6 \times 10^5$ Pa; 3, $P_w = 8 \times 10^5$ Pa. The solid lines correspond to the fast solutions and the slow solutions are represented by the dashed curves.

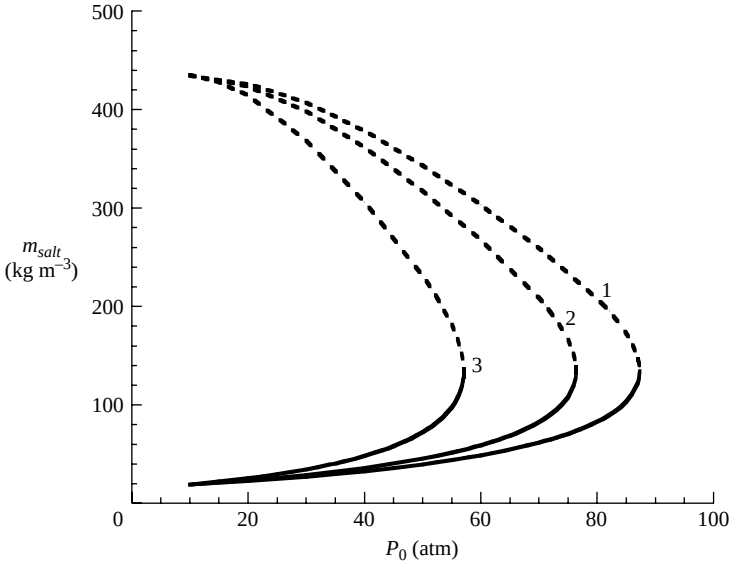

FIGURE 6. Variation of the mass of salt in the solid state in the fracture in the vapour domain, as a function of the far-field reservoir pressure for the different values of the well pressure. $T_0 = 450$ K, $\phi = 0.2$, $c_0 = 0.1$, $\vartheta = 20$: curve 1, $P_w = 4 \times 10^5$ Pa; 2, $P_w = 6 \times 10^5$ Pa, 3, $P_w = 8 \times 10^5$ Pa. The solid lines correspond to the fast solutions and the slow solutions are represented by the dashed curves.

large flow rate is needed to clog up the fracture, but for such flow rates the velocities of the boiling front are small and the effect of front motion is negligible. Therefore, as indicated by equation (2.3), the water flux is approximately equal to the vapour

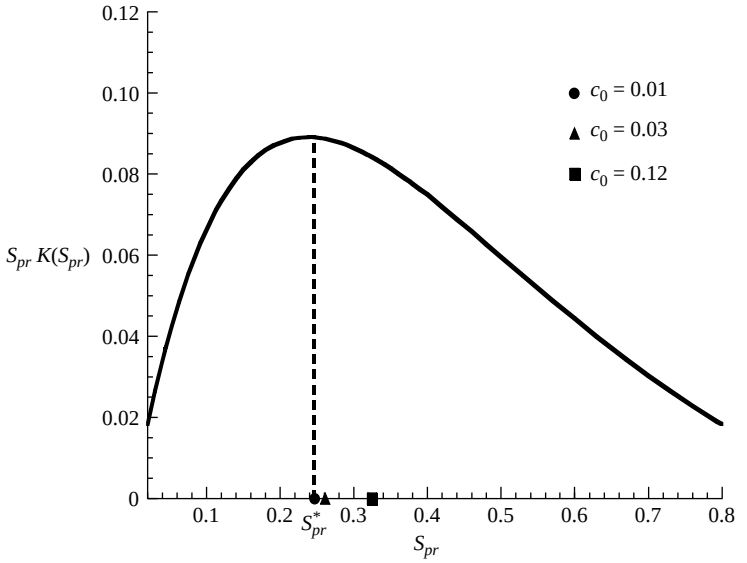

FIGURE 7. Function $S_{pr}K(S_{pr})$ and calculated values of S^*_{pr} for three different initial salt concentrations as shown on the figure.

flux and the computed critical value S^*_{pr} practically coincides with the asymptotic one from criterion (3.19). However, for larger initial salt concentrations, the threshold for blocking occurs at a higher value of S_{pr} as the critical value of salt precipitation becomes larger.

3.4. *Simplified equation for the front velocity*

The system of transcendental equations (3.17) and (3.18) can be reduced to the simple cubic equation for the parameter γ if function $K(S_{pr})$ has the linear form $K(S_{pr}) = 1 - S_{pr}$ and initial salt concentration is not too large. When $P_0 \gg P_f$, the flow rate is large, and it follows from equation (3.17) that $\alpha_w P_f \gamma \ll 1$. Therefore, neglecting the small terms we deduce that system of transcendental equations has the approximate form

$$\left(1 - S_{pr}\frac{\rho_{salt}}{\rho_w}\right)\gamma = -\frac{1}{\sqrt{\pi}}\frac{P_0}{P_f} + \frac{\rho_{v*}}{\rho_w}\,\frac{\mu_w}{\mu_v}\,\frac{1 - S_{pr}}{4\alpha_w P_f \gamma}\,\left(1 - \frac{P_w^2}{P_f^2}\right), \tag{3.20}$$

$$S_{pr} = \frac{\rho_w}{\rho_{salt}} c_0 \left(1 + \frac{1}{\sqrt{\pi}\gamma}\frac{P_0}{P_f}\right). \tag{3.21}$$

Combining these equations, we find that the unknown parameter γ satisfies the cubic equation

$$\gamma^3 + \frac{1}{\sqrt{\pi}}\frac{P_0}{P_f}\,\gamma^2 - G\gamma + G\frac{c_0}{\sqrt{\pi}}\frac{\rho_w}{\rho_{salt}}\frac{P_0}{P_f} = 0, \tag{3.22}$$

where

$$G = \frac{\mu_w}{\mu_v}\frac{\rho_v}{\rho_w}\frac{1}{4\alpha_w P_f}\left(1 - \frac{P_w^2}{P_f^2}\right).$$

In this simplified system, the clogging condition is given by the point of coincidence of two roots of the cubic equation, and this occurs when the discriminant is equal to zero. For comparison, numerical calculations for the exact solution for the clogging point yield $P_0 = 1.364 \times 10^7$ Pa, $\gamma = 0.799$, $S_{pr} = 0.548$. From the cubic equation we have $P_0 = 1.259 \times 10^7$ Pa, $\gamma = 0.753$, $S_{pr} = 0.522$.

4. Influence of salt diffusion on the precipitation process

In the previous section we neglected the effects of salt diffusion and the similarity solution was obtained for the trivial case $c = c_0$. On the following pages we consider the effect of salt redistribution in the liquid phase through molecular diffusion, and show that this leads to the formation of a salt bank in the liquid ahead of the vaporization front. The distribution of the salt concentration ahead of the front can be found from the full equation (3.7). As before, when salt concentration at the boiling front reaches the solubility value then salt precipitates at the front.

The boundary conditions at the vaporization front (3.11) and (3.12) are now supplemented by relations for the solubility as a function of the temperature:

$$c_{sol}(T) = 0.564 - 0.592\frac{T}{373.15} + 0.423\left(\frac{T}{373.15}\right)^2. \tag{4.1}$$

As the temperature in the geothermal reservoir is constant the value of salt concentration at the vaporization front can be found from the relation

$$c_* = c_{sol}(T_0). \tag{4.2}$$

The conservation of salt flux across the vaporization front includes the diffusive flux and has the form

$$\left(S_{pr}\rho_{salt} - c_+\rho_w\right) V_n = -\rho_w c_+ u_{wn+} - \phi D(\text{grad } c)_{n+}. \tag{4.3}$$

The last equation may be rewritten in the form

$$S_{pr} = \frac{\rho_w}{\rho_{salt}} c_+ \left[1 + \frac{k}{\phi\mu_w}\frac{1}{V_n}(\text{grad } P)_{n+} + \frac{D}{V_n c_+}(\text{grad } c)_{n+}\right]. \tag{4.4}$$

4.1. *Similarity solution*

Since the typical length scale for salt diffusion is much smaller than that for pressure adjustment, $L_c \ll L_p$, the salt conservation equation (3.7) may be linearized in the region ahead of the vaporization front (cf. the linearization of the heat equation in Tsypkin & Woods 2004):

$$\frac{\partial c}{\partial t} + \frac{k}{\mu_w}\frac{P_* - P_0}{\sqrt{\pi\kappa_1 t}}\frac{\partial c}{\partial x} = D\frac{\partial^2 c}{\partial x^2}. \tag{4.5}$$

The similarity solution for the salt distribution ahead of the front now takes the form

$$c(\zeta) = c_0 + (c_* - c_0)\frac{\text{erfc}\left[(\zeta + A_c)\sqrt{\kappa/D}\right]}{\text{erfc}\left[(\gamma + A_c)\sqrt{\kappa/D}\right]}, \quad A_c = \sqrt{\frac{\alpha_w}{\pi P_f}}(P_0 - P_*). \tag{4.6}$$

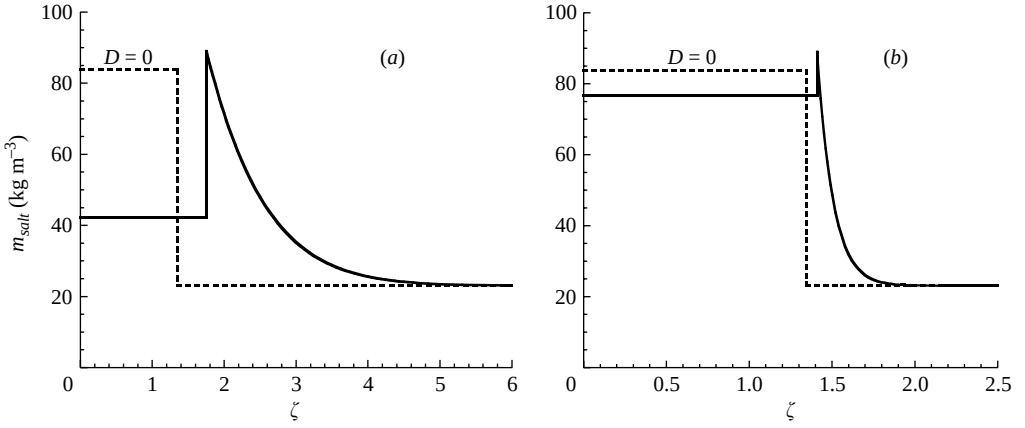

FIGURE 8. Typical distributions of the mass of salt in the water and vapour zones. Solid lines show the mass profiles when salt accumulates ahead of the vaporization front and is redistributed in the liquid phase through molecular diffusion. Dashed lines correspond to the solution without diffusive transport of salt. $T = 450$ K, $c_0 = 0.12$, $P_0 = 7 \times 10^6$ Pa, $P_w = 4 \times 10^4$ Pa. (*a*) $k = 10^{-17}$ m^2, (*b*) $k = 10^{-16}$ m^2

This leads to the following modified transcendental equation for the rate of advance of the boiling front, now including the effects of salt diffusion in the liquid region:

$$S_{pr} = \frac{\rho_w}{\rho_{salt}} c_* \left[1 + \frac{1}{\sqrt{\pi}\gamma} \left(\frac{P_0}{P_f} - 1 \right) \frac{\exp\left(-\gamma^2 \alpha_w^2 P_f^2 \right)}{\operatorname{erfc}(\gamma \alpha_w P_f)} \right] - \frac{\rho_w}{\rho_{salt}} \sqrt{\frac{D}{\pi \kappa}} \frac{c_* - c_0}{\gamma} \frac{\exp(-\gamma^2 \kappa / D)}{\operatorname{erfc}(\gamma \sqrt{\kappa / D})}. \tag{4.7}$$

We have also modified the system of transcendental equations at the front (3.17) and (4.7) for the quantities γ and S_{pr}, that takes into account salt diffusion in the liquid zone.

Figure 8 illustrates the influence of salt diffusion on salt precipitation. For small values of fracture permeability (figure 8*a*) the diffusive flux of salt has the same order of magnitude as the advective flux from the far field. Therefore a substantial mass of salt which is advected towards the boiling front from the far field accumulates in a bank of high-concentration liquid ahead of the vaporization front, and the mass of salt which actually precipitates at the boiling front is reduced. However, for larger values of the fracture permeability, the rate of advection from the far field also increases, and so the role of salt diffusion decreases (figure 8*b*). Eventually, if the permeability is larger than about 10^{-16} m^2 then the influence of salt diffusion on the process is negligible.

Figure 9 illustrates the influence of salt diffusion in the liquid on the vaporization rate. Three curves are shown: a reference curve in which the diffusivity is set to zero (cf. § 3); and curves for which the fracture has permeability 10^{-16} and 10^{-17}. Since the salt diffusion reduces the mass of precipitate for a given liquid flux from the far field, we expect the speed of the fast boiling front regime to increase for a given reservoir pressure, since the matrix between the well and the front has less precipitate and therefore has a higher permeability. Similarly, with the slow boiling front regime, the diffusion of salt into the bank ahead of the boiling front leads to a smaller mass of precipitate in the matrix; therefore for a given reservoir pressure, and hence flow rate, the boiling front can advance more slowly without the matrix becoming fully clogged.

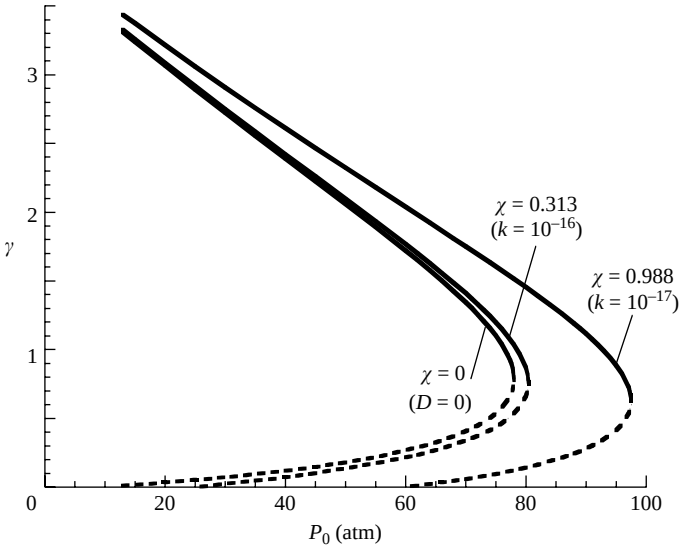

FIGURE 9. Variation of the dimensionless velocity of the front as a function of the reservoir pressure for the different values of the dimensionless parameter χ which represents the ratio of the diffusive transport of salt to the advective transport of salt. $T_0 = 450$ K, $\phi = 0.2$, $c_0 = 0.12$, $P_w = 4 \times 10^5$ Pa. The solid lines represent the fast solutions and the slow solutions are represented by the dashed curves.

As a result of this change in the speed of the boiling front for both regimes, the critical reservoir pressure at which the two regimes coincide, and hence the fracture will clog up, also increases.

Figure 10 illustrates how the critical reservoir pressure at which the similarity solutions cease to exist depends on the initial concentration of salt in the fluid. Three curves are given corresponding to the case in which salt diffusion is neglected ($\chi = 0$) as appropriate for a somewhat higher permeability fracture, and for two cases in which the salt diffusion is included, and the fracture permeability has values 10^{-16} and 10^{-17} m^2. For higher salt concentrations, there is more precipitation on boiling and hence the maximum reservoir pressure for which similarity solutions exist is smaller. The figure also shows how in low-permeability fractures, in which salt diffusion leads to banking of salt ahead of the boiling front, the range of reservoir pressures for which similarity solutions exist increases.

5. Salt precipitation in permeable rock

For completeness, in this section we briefly turn from isothermal fracture flow and extend the analysis to consider evaporation in a laterally extensive permeable rock. In this case there is no significant lateral heat conduction. Instead, the heat required for vaporization originates ahead of the boiling front as in the study of Tsypkin & Woods (2004). However, as for the case of the fracture flow described in § 3, the process of salt precipitation has a fundamental influence on the conditions for the existence and uniqueness of the similarity solution. Indeed, we now show that by analogy with the fracture problem, if salt precipitation occurs in tandem with the boiling, then two different regimes may develop: the slow boiling front mode, and the fast boiling front mode.

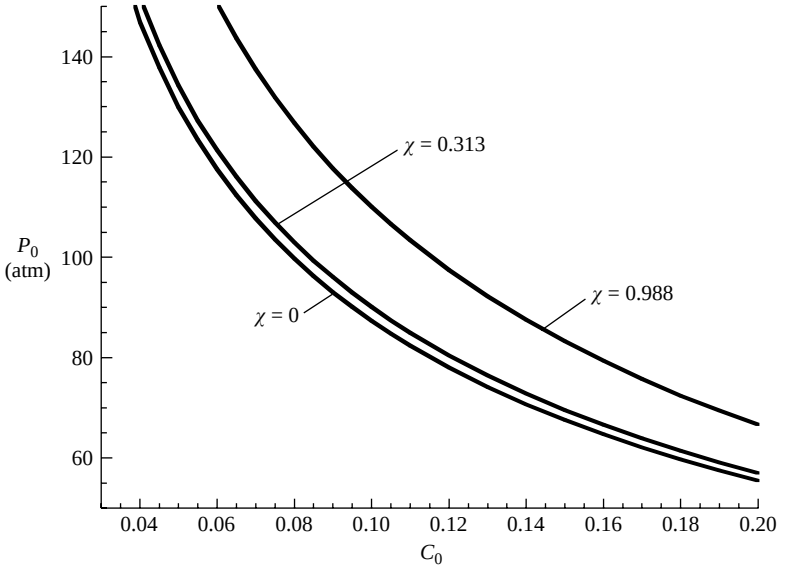

FIGURE 10. Critical diagram shows the maximum reservoir pressure as a function of the initial salt concentration for which a similarity solution exits. Three curves are shown corresponding to the three values of the parameter χ. $T_0 = 450$ K, $\phi = 0.2$; $P_w = 4 \times 10^6$ Pa. Below the critical curves salt precipitates at the boiling front and above the critical curves the high advective flux of salt leads to the clogging of the fracture.

5.1. *Model formulation*

The temperature distribution in the water-saturated permeable porous rock is given from the conservation of energy. Combining the energy conservation equation with Darcy's law we obtain

$$(\rho C)_1 \frac{\partial T}{\partial t} - \frac{k}{\mu_w} \rho_w C_w \text{grad } P \text{ grad } T = \lambda_1 \Delta T \tag{5.1}$$

where $\lambda_1 = \phi\lambda_w + (1-\phi)\lambda_s$ and $(\rho C)_1 = \phi\rho_w C_w + (1-\phi)\rho_s C_s$ with C representing the specific heat, and λ the thermal conductivity, while the subscripts s and w refer to properties of the porous matrix and water respectively.

As the temperature in the vapour region is constant the conservation of energy across the vaporization front has the form

$$\phi q \rho_w V_n = \lambda_+ (\text{grad } T)_{n+} - \frac{kq\rho_w}{\mu_w} (\text{grad } P)_{n+} \tag{5.2}$$

where q is the specific heat of vaporization.

To solve the equations for heat transfer (5.1) for the one-dimensional problem we apply the initial condition for the temperature field

$$t = 0 : \; T = T_0. \tag{5.3}$$

As there is no heat sink in the vapour region the fluid reaches the well-bore in the vapour state and the temperature throughout the vapour region has a constant value which is equal to the vaporization temperature T_* at the front.

5.2. *Similarity solution*

As shown by Tsypkin & Woods (2004), owing to the large difference between the typical length scales for temperature and pressure variations, the nonlinear heat

conservation equation may be linearized in the region ahead of vaporization front

$$\frac{\partial T}{\partial t}+\frac{\rho_w C_w}{(\rho C)_1}\frac{k}{\mu_w}\frac{P_*-P_0}{\sqrt{\pi\kappa_1 t}}\frac{\partial T}{\partial x}=a_1\frac{\partial^2 T}{\partial x^2},\quad \text{where}\quad a_1=\frac{\lambda_1}{(\rho C)_1},\tag{5.4}$$

and the similarity solution for the temperature has the form

$$T(\zeta)=T_0+(T_*-T_0)\frac{\operatorname{erfc}((\zeta+A_T)\sqrt{\kappa/a_1})}{\operatorname{erfc}((\gamma+A_T)\sqrt{\kappa/a_1})},\quad A_T=\frac{\phi\rho_w C_w}{\sqrt{\pi}(\rho C)_1}\frac{P_0}{P_f}\left(1-\frac{P_0}{P_*}\right).\tag{5.5}$$

Substituting solution (5.5) into the relation for the conservation of heat at the front (5.2) we obtain

$$\gamma+\frac{P_0}{\sqrt{\pi}P_f}\left(1-\frac{P_*}{P_0}\right)\frac{\exp(-\gamma^2\alpha_w^2P_f^2)}{\operatorname{erfc}(\gamma\alpha_w P_f)}-\frac{\lambda_1 T_0}{\phi q\rho_w}\frac{1}{\sqrt{\pi a_1\kappa}}\left(1-\frac{T_*}{T_0}\right)\frac{\exp(-(\gamma+A_T)^2\kappa/a_1)}{\operatorname{erfc}((\gamma+A_T)\sqrt{\kappa/a_1})}=0.\tag{5.6}$$

As the vaporization temperature T_* at the front is an unknown parameter then equation (5.6) is supplemented by the relation

$$c_*=c_{sol}(T_*)\tag{5.7}$$

and the modified Clausius–Clapeyron relation in which we account for the dependence of the salt concentration on the vaporization temperature:

$$\ln\frac{P_*}{P_a}=A+\frac{B}{T_*-\alpha c_*}.\tag{5.8}$$

Here, for example, for sodium chloride $\alpha=20$.

As a result we obtain the system of five transcendental equations (3.17), (4.7), (5.6), (5.7) and (5.8) for the unknown parameters γ, c_*, P_*, T_* and S_{pr}.

These equations have been solved numerically. The general structure of the solution is analogous to those found by Tsypkin & Woods (2004) except that now there is a bank of salt ahead of the boiling front, as described herein for the fracture problem. However, the precipitation of the salt in the zone between the well and the boiling front leads to a nonlinearity as in the fracture problem, and so a slow and a fast boiling front regime can both develop.

Figure 11 illustrates the variation of the mass of precipitate in the porous matrix as a function of the reservoir pressure, as predicted by the model. The figure illustrates the two solution branches for both the case in which the diffusion of salt is neglected (curve 1) and in which the diffusion of salt is included (curve 2). Curve 1 corresponds to the case of a relatively high-permeability porous layer, in which case no significant salt bank develops ahead of the boiling front. Curve 2 illustrates the decrease in the mass of precipitate in the fast front regime and the increase in the mass of precipitate in the slow front regime as a result of the salt bank. This effect is directly analogous to the effect of salt diffusion in the fracture boiling problem discussed earlier.

6. Discussion

In this work we have explored the problem of decompression-driven boiling of an aqueous solution in a high-pressure hot fractured rock. We have found a class of similarity solutions for the isothermal problem of flow in a fracture, in which heat supplied from neighbouring impermeable rock maintains an approximately constant

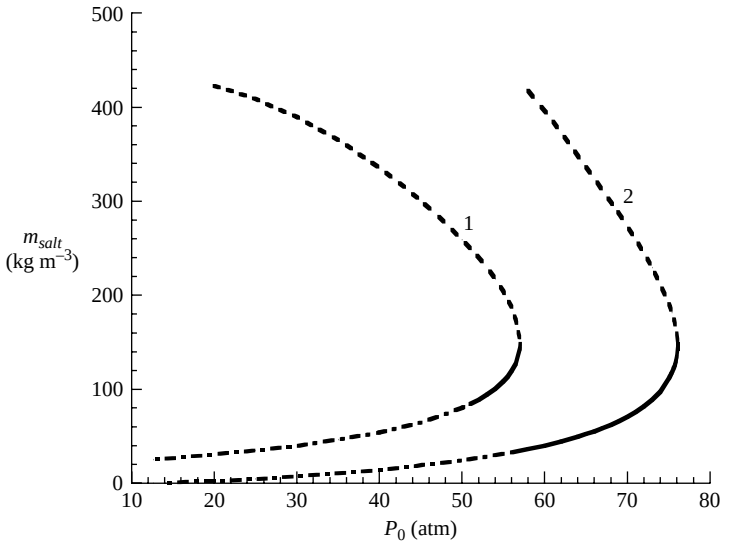

FIGURE 11. Comparison of the model predictions of salt precipitation in a porous rock, with a planar vaporization front, for different reservoir pressures. In the calculations, $T_0 = 450$ K, $\phi = 0.2$; $P_w = 4 \times 10^6$ Pa, $k = 10^{-17}$ m^2. Curve 1 corresponds to the case in which we neglect the effects of salt diffusion, which is appropriate for a relatively large permeability; curve 2 corresponds to a calculation in which we include the effects of salt diffusion, which is important in forming a bank of high-salinity water ahead of the boiling front and thereby suppressing salt precipitation in a lower-permeability rock. The dashed lines represent the slow solutions. The solid parts of the curves denote the fast solutions in which there is no superheating of water ahead of the front. The dot-dashed parts of the curves represent those fast solutions for which there is some superheating in the liquid.

temperature in the fracture. Our analysis has established that if there is some salt precipitation associated with the boiling of the liquid, there are two possible branches for the self-similar solution. Further, these two branches coincide at a critical value of the liquid flux, and for liquid fluxes in excess of this value, the self-similar solutions cease to exist. Instead, the rock becomes clogged with salt. This result is in sharp contrast to the case with no precipitation, in which there is a unique flow solution, and the self-similar flow regime can develop for arbitrarily large liquid fluxes advancing towards the well. We have extended the analysis to the case in which a boiling front migrates through a hot porous rock and precipitates salt. Although the analysis is more involved, a directly analogous result arises: for low liquid flow rate, two self-similar solution branches are possible, while above a particular flow rate at which the branches coincide, the solutions cease to exist.

Multi-valued solutions appear in many branches of mathematical physics and we need some additional constraints to determine which solution will arise in practice. In the limit of zero salt concentration, the fast flow solution coincides with the simpler problem of pure water vaporization (Tsypkin & Woods 2004). Also, as for the case of the vaporization of pure water (Tsypkin & Woods 2004), if the reservoir pressure increases then, with the fast solution, the speed of the boiling front decreases. In contrast, with the slow solution, the front velocity increases with reservoir pressure. Furthermore, for the fast solution, the mass of precipitate increases with initial salt concentration whereas it is predicted to decrease in the slow solution. These properties

suggest that the fast solution is stable while the slow solution is unstable, and so we expect the fast solution to arise in practice.

The results have some important implications for the formation and sealing of fractured rock by convection in high-temperature geothermal or hydrothermal systems involving phase change. In particular, the result implies that a self-similar boiling flow can only develop if the source rock has relatively low pressure, for example in shallower systems, in which the liquid flow rate is limited owing to the relatively low pressures. In deeper systems, with the same background permeability, the pressure is typically higher, and the self-similar flow may not be possible; instead any boiling might lead to sealing up of the fracture by the precipitation induced by the boiling. Thus in a general sense, we might expect fumaroles and other examples of natural vapour venting from a permeable rock to be associated with the shallower parts of the system.

It was shown in Tsypkin & Woods (2004) that the decrease in temperature at the boiling front may lead to the development of superheat in the water ahead of the front. However, in a fractured system, where the flow is dominated within the fractures, there may be sufficient heat flux from the surrounding rock that to leading order the temperature of the fluid remains fixed. In this case, the liquid ahead of the phase transition front does not become superheated. In turn this can suppress the formation of any two-phase zone ahead of the front.

We are grateful for funding from the BP Institute which supported G. T. as a senior visiting fellow.

REFERENCES

Battistelli, A., Calore, C & Pruess K. 1995 Analysis of salt effects on the depletion of fractured reservoir blocks. *World Geothermal Congress, 1995, Florence, Proc.*, pp. 1613–1618.

Battistelli, A., Calore, C. & Pruess K. 1997 The simulator TOUGH2/EWASG for modelling geothermal reservoirs with brines and a noncondensible gas. *Geothermics.* **26**, 437–464.

Phillips, O. M. 1991 *Flow and Reactions in Permeable Rocks.* Cambridge University Press.

Tsypkin, G. G. & Woods A. W. 2004 Vapour extraction from a water saturated geothermal reservoir. *J. Fluid Mech.* **506**, 315–330.